
**ORDER, DISORDER, AND PHASE TRANSITION
IN CONDENSED SYSTEM**

μ SR Study of $\text{Eu}_{0.8}\text{Ce}_{0.2}\text{Mn}_2\text{O}_5$ and EuMn_2O_5 Multiferroics

**S. I. Vorob'ev^{a,*}, D. S. Andrievskii^a, S. G. Barsov^a, A. L. Getalov^a, E. I. Golovenchits^b,
E. N. Komarov^a, S. A. Kotov^a, A. Yu. Mishchenko^c, V. A. Sanina^b, and G. V. Shcherbakov^a**

^a Petersburg Nuclear Physics Institute, National Research Center Kurchatov Institute,
Gatchina, Leningradskaya oblast, 188300 Russia

^b Ioffe Physical–Technical Institute, Institute, Russian Academy of Sciences,
St. Petersburg, 194021 Russia

^c National Research Nuclear University MEPhI (Moscow Engineering Physics Institute),
Moscow, 115409 Russia

* e-mail: vsilova@npfi.spb.ru

Received July 23, 2015; in final form, July 6, 2016

Abstract—A comparative μ SR study of ceramic samples of the EuMn_2O_5 and $\text{Eu}_{0.8}\text{Ce}_{0.2}\text{Mn}_2\text{O}_5$ multiferroics is performed in the temperature range from 15 to 300 K. It is found that the Ce doping of the EuMn_2O_5 sample slightly reduces the temperature of the magnetic phase transition from $T_N = 45$ K for the EuMn_2O_5 sample to $T_N = 42.5$ K for the $\text{Eu}_{0.8}\text{Ce}_{0.2}\text{Mn}_2\text{O}_5$ sample. Below the temperature T_N for both samples, there are two types of localization of a thermalized muon with different temperature dependences of the precession frequency of the magnetic moment of the muon in an internal magnetic field. The higher frequency in both samples refers to the initial antiferromagnetic matrix. The behavior of this frequency in $\text{Eu}_{0.8}\text{Ce}_{0.2}\text{Mn}_2\text{O}_5$ follows the Curie–Weiss law with the exponent $\beta = 0.29 \pm 0.02$, which differs from the value $\beta = 0.39$ standard for 3D Heisenberg magnetism and is observed in EuMn_2O_5 , because of the strong frustration of the doped sample. The temperature-independent low frequency is due to the presence of $\text{Mn}^{3+}\text{–Mn}^{4+}$ ferromagnetic pairs located along the b axis of the antiferromagnetic matrix and in the regions of phase separation, which contain such ion pairs and e_g electrons recharging them. In both samples, polarization losses are the same (about 20%) and are associated with the formation of $\text{Mn}^{4+}\text{–Mn}^{4+} + \text{Mu}$ complexes near $\text{Mn}^{3+}\text{–Mn}^{4+}$ ferromagnetic pairs. In the temperature interval from 25 to 45 K, the separation of the $\text{Eu}_{0.8}\text{Ce}_{0.2}\text{Mn}_2\text{O}_5$ structure into two fractions where the relaxation rates of polarization of muons differ by an order of magnitude is revealed. This effect is due to a change in the state of regions of phase separation (1D superlattices) at the indicated temperatures. Such effect in EuMn_2O_5 is significantly weaker.

DOI: 10.1134/S1063776116130215

1. INTRODUCTION

Manganites RMn_2O_5 (R is a rare-earth element) are the typical representatives of multiferroics where ferroelectric ordering at $T < T_C \approx 30\text{--}35$ K is induced by magnetic ordering with $T_N \approx 40\text{--}45$ K and a strong magnetoelectric interaction exists [1, 2]. The possibility of controlling the electric (magnetic) properties by applying a magnetic (electric) field attracts attention to such multiferroics. It was previously accepted that RMn_2O_5 manganites have orthorhombic symmetry with the space group $Pbam$ [3]. The charge ordering of manganese ions with variable valence along the b axis at the appearance of a magnetic order results in the appearance of noncentrosymmetry and ferroelectricity owing to exchange striction [4]. Recent detailed structural study [5] shows that RMn_2O_5 compounds have the noncentrosymmetric space group Pm , which allows the existence of electric polarization in

RMn_2O_5 at room temperature. Monoclinic distortions revealed in [5] were weak against the background of the space group $Pbam$. The authors of [5] did not doubt the experimentally well-established magnetic properties and the existence of magnetically induced ferroelectricity in RMn_2O_5 . They believed that the low-temperature polar order coexists with a high-temperature electric polarization of a different nature and enhances it. We recall that the μ SR method gives information on the magnetic state of a crystal and our results are in agreement with the low-temperature magnetic properties described within the space group $Pbam$.

The unit cell of RMn_2O_5 contains one Mn^{3+} ion and one Mn^{4+} ion and the distribution of these ions in the crystal (charge ordering) plays a key role in the establishment of its properties. There are two types of charge ordering in RMn_2O_5 . The first type is due to

the alternation of ferromagnetic and antiferromagnetic Mn^{3+} – Mn^{4+} ion pairs along the b axis. The difference between indirect antiferromagnetic exchange between antiferromagnetic pairs and double exchange between ferromagnetic pairs results in exchange striction inducing electric polarization along the b axis at $T < 30$ – 35 K [4]. The second type of charge ordering is due to the distribution of ions in layers perpendicular to the c axis [3]. Mn^{4+} ions occupy the $z = 0.25c$ and $(1 - z) = 0.75c$ sites in the octahedral oxygen environment (MnO_6); Mn^{3+} ions are at the $z = 0.5c$ sites in pentagonal pyramids (MnO_5); and R^{3+} ions occupy the $z = 0$ site. Charge ordering along the c axis is due to the processes of phase separation and self-organization of charge carriers, which are characteristic of all manganites containing the Mn^{3+} and Mn^{4+} ions [6, 7]. Phase separation leads to the formation of limited ferromagnetic conducting regions inside the dielectric antiferromagnetic (paramagnetic) matrix of the initial crystal because phase separation is energetically favorable. Dynamically equilibrium regions of phase separation are formed at the balance of strong attractions of the charge carriers (double exchange, distortion of the lattice) and their Coulomb repulsion [6, 7]. For this reason, phase separation exists from low temperatures up to those above room temperature.

The magnetic and dielectric properties of $\text{Eu}_{0.8}\text{Ce}_{0.2}\text{Mn}_2\text{O}_5$ (ECMO) and EuMn_2O_5 (EMO) were studied in [8, 9]. Doping by Ce^{4+} substituting the sites of R^{3+} ions did not change the symmetry of the crystal and slightly affected the cell parameters, but increased the concentration of regions of phase separation as compared to the initial crystal. Indeed, in both crystals, e_g electrons from Mn^{3+} ions located in the $z = (1/2)c$ layers can tunnel to Mn^{4+} located in the $z = (1/4)c$ and $z = (3/4)c$ layers. As a result, Mn^{3+} – Mn^{4+} ferromagnetic pairs and electrons recharging them appear in all layers occupied by manganese ions. An additional source of electrons appears in doped crystals and these electrons enter the same Mn-ion layers. In ECMO, Ce^{4+} ions partially substitute Eu^{3+} ions, forming extra electrons, which recharge manganese ions in the neighboring planes. As a result of phase separation, charge carriers and Mn^{3+} – Mn^{4+} ferromagnetic pairs form conducting ferromagnetic regions inside layers perpendicular to the c axis. These regions are arranged opposite each other along the c axis, thus forming 1D superstructures. The volume of regions of phase separation and their internal structure depend on the temperature. The layered structure of regions of phase separation along the c axis at room temperature was observed in precision X-ray diffraction studies both in EMO and in ECMO [8, 9]. The period of superstructures in these crystals was 900 and 700 Å, respectively. In this case, the volumes of the initial paramagnetic dielectric matrix and ferromagnetic conducting layers were comparable. At low tem-

peratures ($T < 40$ K), superstructures had the form of 1D superlattices with alternating ferromagnetic insulating and conducting layers. Such superlattices are located far from each other in the antiferromagnetic insulating matrix [10, 11]. The study of the heat capacity of ECMO showed that the same series of phase transitions as in EMO is observed at low temperatures [8]. This indicates that the doping-modified volume in ECMO is small at such temperatures. The magnetic resonance studies of the ECMO and EMO crystals [10, 11] showed that a similar set of ferromagnetic resonances from individual layers of superlattices is observed at temperatures $T < 40$ K in both crystals, but the intensities of signals in ECMO are much higher than those in EMO. This indicates that the properties of individual regions of phase separation in these crystals are similar but the concentrations of these regions in these crystals are different.

The main aim of this work is the comparative μSR study of the magnetic properties of the ECMO and EMO compounds. The time spectra of positrons from the decay of muons stopped in samples were recorded in zero external magnetic field in the temperature range from 15 to 300 K. The temperature dependences of the parameters of relaxation of the polarization of the muon, precession frequencies of its spin in the internal magnetic fields of samples, and partial contributions from various precession modes to the total asymmetry of decay of muons were obtained from these spectra. We revealed difference in the behavior of the parameters of relaxation and total asymmetry in EMO and ECMO in the temperature range of 25–45 K, which is due to difference in the concentrations of regions of phase separation in these crystals. The μSR method was previously used to study the properties of undoped multiferroics EuMn_2O_5 [12] and GdMn_2O_5 [13]. It was found that the polarization of muons was not conserved below the temperature of the transition T_N of the studied samples to a magnetically ordered state. Maxima of the relaxation parameters were also observed near this temperature. An important role of processes of charge transfer between Mn^{3+} – Mn^{4+} ion pairs in the formation of the long-range magnetic order in these multiferroics was revealed.

2. EXPERIMENT

The measurements were performed at the μSR setup placed at the output of the muon channel of the PNPI synchrocyclotron [14]. We used a beam of positive muons with the momentum $p_\mu = 90$ MeV/ c , relative momentum spread $\Delta p_\mu/p_\mu$ (FWHM) = 0.02, and longitudinal polarization $P_\mu \sim 0.90$ – 0.95 . Muons stopped in targets, which were containers with ceramic samples. Both studied cylindrical samples had a diameter of 30 mm and a thickness of 12 mm and were fabricated by solid-phase synthesis technology. The

structure of these ceramic samples (space group *Pbam*) was determined by the X-ray diffraction study, which confirmed that they are single-phase. The sizes of ceramic grains were several tens of microns. The samples were placed in a cryostat, which allowed maintaining the temperature in the range of 15–300 K with an accuracy of about 0.5 K.

Measurements were performed in three regimes of cooling (heating) of the samples. The first regime (RUN1) involved the cooling of a sample from the temperature $T \approx 290$ K to $T = 41$ K with stops at intermediate temperature points with the step $\Delta T \approx 5$ – 10 K, where data were collected for two hours in the temperature stabilization regime. Then, the sample was cooled quite rapidly (in about 1 h) from 41 to 15 K; after that, the sample was stepwise heated to the final temperature $T = 40$ K (with a step of $\Delta T \approx 2.5$ K) with the collection of data at each intermediate stabilized-temperature point. This cooling regime was applied to both samples. The second regime (RUN2) involved fast (in about 1 h) cooling from $T = 290$ K to $T = 15$ K and subsequent heating with stops at given temperatures for the collection of data (for about 6 h at each temperature). This regime was applied only to the ECMO sample. The third regime (RUN3) included fast (in about 1 h) cooling of the sample to a temperature of about 70 K and subsequent stepwise cooling to $T = 15$ K with stops at given temperatures with the step $\Delta T = 5$ K for the collection of data (for about 2 h at each temperature). Then, the sample was heated from the temperature $T = 17.5$ K to the final temperature $T \approx 75$ K with stops at intermediate temperatures with the step $\Delta T = 5$ K for the collection of data (for about 2 h at each temperature). The regime RUN3 was applied only to the ECMO sample.

Time spectra of decay positrons were measured in two time intervals (10 and 1.1 μs) with a step of about 5 ns/channel and 0.8 ns/channel, respectively. The time spectra were described by the expression

$$N_e(t) = N_0 \exp(-t/\tau_\mu) [1 + a_s G_s(t) + a_b G_b(t)] + B, \quad (1)$$

where N_0 is the normalization constant proportional to the number of detected positrons; τ_μ is the muon lifetime; a_s and a_b are the partial contributions to the observed asymmetry of positrons from the decay of muons stopped in the sample and in the construction elements of the setup, respectively; $G_s(t)$ and $G_b(t)$ are the respective polarization relaxation functions; and B is the background of random coincidences. The magnitude and time structure of the background of random coincidences were determined from the processing of the initial segment of the time spectrum preceding the instant of muon stop in the sample. Asymmetry a_b for each sample was extracted from the processing of time spectra recorded in an external magnetic field at the temperature of samples below the Néel temperature ($T < T_N$). In this case, the observed amplitude of the precession frequency in a given external magnetic field is equal to the contribution a_b to the

total asymmetry. The same processing provides the relaxation rate of the polarization of muons λ_b stopped in the construction elements. The spectra measured in zero external magnetic field were processed with the following relaxation function of the background component: $G_b(t) = \exp(-\lambda_b t)$. For the studied ceramic samples, $a_b \approx 0.02$, whereas the total asymmetry is $a_F = a_s + a_b \approx 0.3$. Asymmetry a_F is equal to the amplitude of muon-spin precession in the external magnetic field at the temperature of the sample above the Néel temperature T_N . In the paramagnetic region, the asymmetry of decay of muons stopped in the sample $a_s = a_F - a_b$ is constant a_0 . The observed residual asymmetry a_s can depend on the temperature if additional channels of loss of the polarization in the sample are involved as the temperature varies.

The experimental data were processed under the standard assumption that the relaxation function is factorized:

$$G_s(t) = G_{st}(t)G_d(t). \quad (2)$$

The dynamic relaxation function $G_d(t) = \exp(-\lambda t)$ describes average spatial fluctuations of internal magnetic fields in the sample at large distances (about the muon diffusion length). The form and parameters of the static relaxation function $G_{st}(t)$ are determined by the distribution of local magnetic fields in the regions preferable for the localization of a muon after its deceleration in the sample and end of the process of its thermalization. Such a representation of the relaxation function $G_s(t)$ is valid if the dynamic relaxation rate is much lower than the relaxation rate associated with the fluctuation of local static magnetic fields. This condition is satisfied in the studied samples in almost the entire temperature range where measurements were performed.

The static relaxation function for an isotropic ferromagnet (antiferromagnet) in zero external magnetic field can be represented in the form

$$G_{st}(t) = \sum_i a_i \left[\frac{1}{3} + \frac{2}{3} \cos(\Omega_i t) \exp(-\Delta_i t) \right]. \quad (3)$$

Here, a_i are the partial amplitudes of the observed muon spin precession frequencies $\Omega_i = 2\pi F_i$ in the local internal magnetic field. The static relaxation rates Δ_i depend on the space fluctuations of these fields at the points of localization of muons in the sample. The term 1/3 in the square brackets corresponds to the fraction of the longitudinal component in the orientation of the internal magnetic fields with respect to the direction of the muon spin, whereas the term with a coefficient of 2/3 corresponds to the transverse component in the orientation of the internal magnetic fields with respect to the direction of the muon spin. In the limiting case of the paramagnetic state, $G_{st}(t) = 1$.

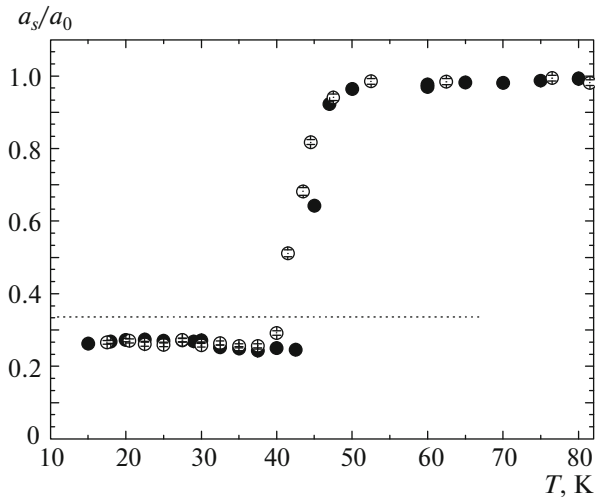


Fig. 1. Temperature dependence of normalized residual asymmetry for the (open circles) ECMO and (closed circles) EMO samples in the RUN1 regime. The horizontal dotted straight line marks the $a_s/a_0 = 1/3$ level.

Using Eqs. (1)–(3) and taking into account the condition $\lambda \ll \Delta$, temperature dependences of the parameters of the relaxation function of polarization of muons stopped in each sample can be determined from experimental time spectra.

3. RESULTS AND DISCUSSION

Figures 1 and 2 show the residual asymmetry a_s divided by a_0 (residual asymmetry in the paramagnetic region) and the relaxation rate λ for the ECMO and EMO samples in the regime RUN1. At temperatures $T \geq 80$ K, the parameters a_s and λ become constant (up to a temperature of 290 K) and, for this reason, are not shown in Figs. 1 and 2. A jump of the relative residual asymmetry a_s/a_0 and the maximum of the relaxation rate λ correspond to the temperature of establishment of the long-range magnetic order $T_N \approx 45$ K for the EMO sample [12] and $T_N \approx 42.5$ K for the ECMO sample.

It is noteworthy that measured asymmetry a_s for an isotropic magnet in the magnetic ordering region is equal to $a_0/3$.

The relaxation rates and polarization loss, which is about 20% ($a_s/a_0 < 1/3$), below the magnetic ordering temperature T_N for the EMO and ECMO samples appeared to be close at any cooling regime. Polarization loss is due to the fast depolarization of some muons during a time shorter than 9 ns (dead time of the detection system). Fast depolarization occurs because of formation of $\text{Mn}^{4+}-\text{Mn}^{4+} + \text{Mu}$ ferromagnetic complexes (where Mu is the muonium, i.e., the μ^+e^- bound state). Such complexes appear owing to the spin–spin interaction of a muon μ^+ with polarized

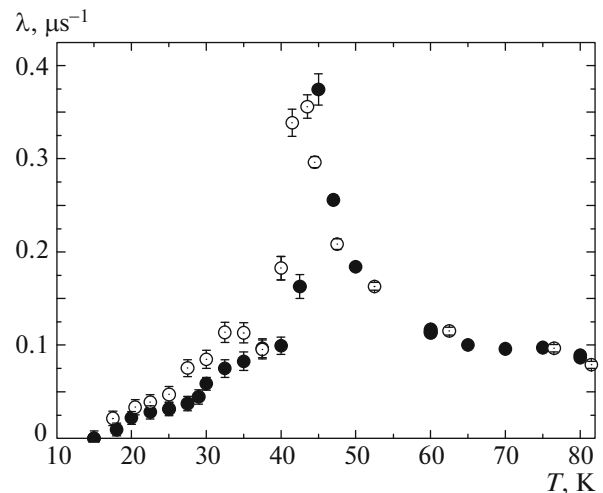


Fig. 2. Temperature dependence of the relaxation rate of the polarization of muons stopped in the (open circles) ECMO and (closed circles) EMO samples in the RUN1 regime.

e_g electrons involved in double exchange in $\text{Mn}^{3+}-\text{Mn}^{4+}$ ferromagnetic pairs. Such ion pairs in EMO exist in the basic antiferromagnetic matrix along the b axis (at $T < T_N$) and in the regions of phase separation (existing in a wide temperature interval of 5–300 K [8, 9]). An additional channel of the formation of $\text{Mn}^{3+}-\text{Mn}^{4+}$ ferromagnetic pairs existing in the ECMO sample because of electron doping increases the volume of the sample with phase separation. However, doping simultaneously partially destroys the charge order along the b axis at $T < T_N$, reducing the number of such pairs in the basic antiferromagnetic matrix. As a result, polarization losses in EMO and ECMO at $T < T_N$ are almost identical.

Figure 3 shows the relaxation rate λ for ECMO in three regimes of cooling (heating). Only for the regime RUN2, the satisfactory description of time spectra in the temperature range of 25–40 K requires an additional dynamic term in the $N_e(t)$ function (1) in the form $a_{s2}G_{d2}(t) = a_{s2}\exp(-\lambda_2 t)$:

$$N_e(t) = N_0 \exp(-t/\tau_\mu) \times [1 + a_s G_s(t) + a_{s2} G_{d2}(t) + a_b G_b(t)] + B, \quad (4)$$

where a_{s2} and λ_2 are the partial asymmetry and relaxation rate of the polarization of muons in the additional depolarization channel, respectively. Thus, the ordered antiferromagnetic and disordered paramagnetic phases coexist in this temperature range.

Figure 4 demonstrates that the characters of relaxation of the polarization of muons are different in the temperature range of 25–40 K ($T = 37.5$ K) and beyond it ($T = 17.5$ K and $T = 70$ K). For better repre-

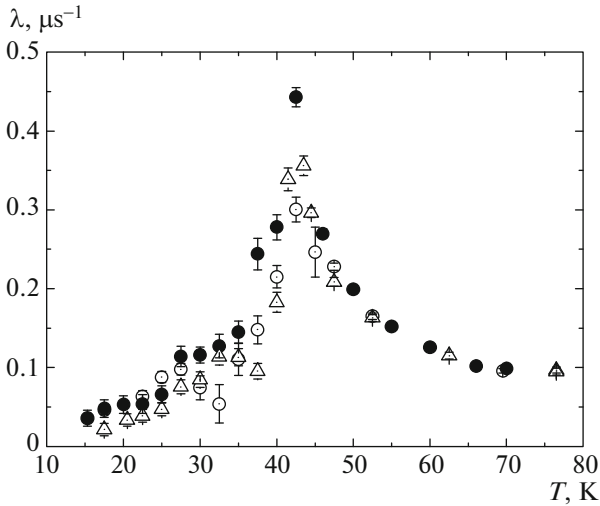


Fig. 3. Temperature dependence of the relaxation rate of the polarization of muons stopped in the (open circles) ECMO and (closed circles) EMO samples in the (triangles) RUN1, (open circles) RUN2, and (closed circles) RUN3 regimes.

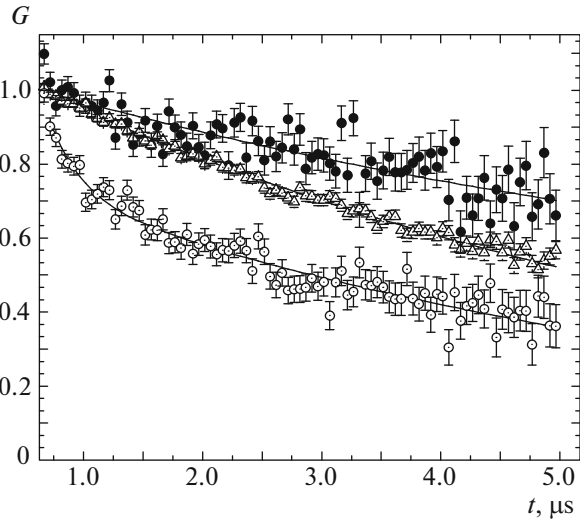


Fig. 4. Relaxation functions $G_d(t)$ at temperatures $T =$ (triangles) 70, (open circles) 37.5, and (closed circles) 17.5 K in the RUN2 regime.

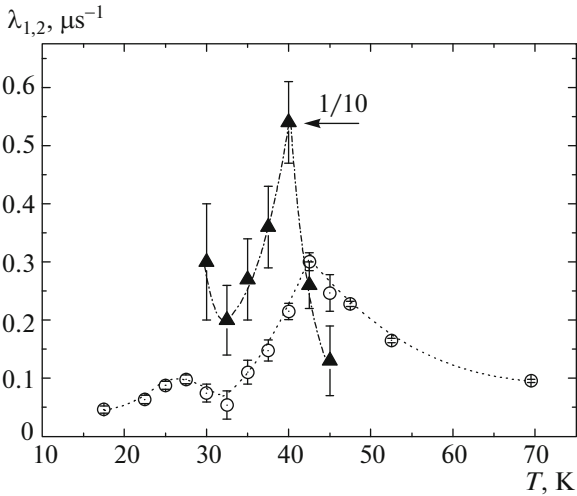


Fig. 5. Effect of the separation of the ECMO sample in the relaxation rates of the polarization of muons in the RUN2 measurement regime: (open circles) slowly relaxing component (λ_1) and (triangles) rapidly relaxing component ($\lambda_2/10$ is plotted).

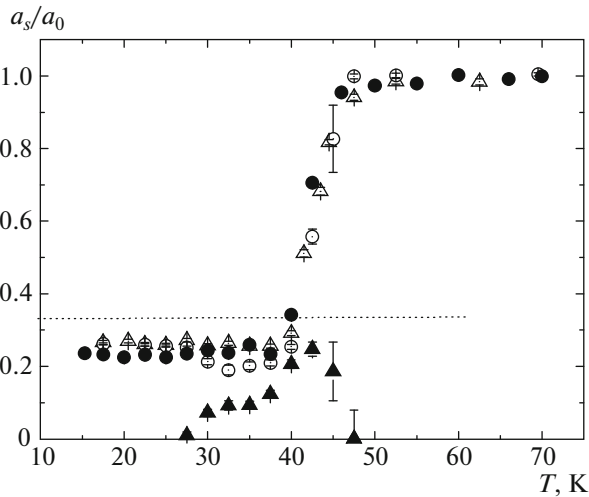


Fig. 6. Temperature dependences of the normalized residual asymmetry in the ECMO sample for the (open triangles) RUN1 and (closed circles) RUN3 regimes and (open circles) slowly relaxed and (closed triangles) rapidly relaxed components in the RUN2 regime. The dotted horizontal straight line is the $a_s/a_0 = 1/3$ level.

sentation, the time spectra were summarized over ten channels (about 50 ns/channel). It is seen in Fig. 5 that the relaxation rate λ_2 is an order of magnitude higher than the relaxation rate λ_1 .

Figure 6 demonstrates the fraction of muons stopped in the regions of the sample with such a fast dynamics in the observation time. The total residual asymmetry in the regime RUN2 in the range of 25–45 K is $3a_s/a_0 + a_{s2}/a_0$.

Below the Néel temperature $T_N = 42.5$ K, the same anomalies of magnetization that correspond to a series of low-temperature magnetic phase transitions observed in EMO are detected in the basic volume of the doped crystal [9]. A long-range magnetic order with an incommensurate phase is established in the range 35–42.5 K. The transition of the sample to a state with a commensurate phase occurs in the temperature range of 22–35 K. For this reason, the fast dynamics observed in the temperature range of 25–

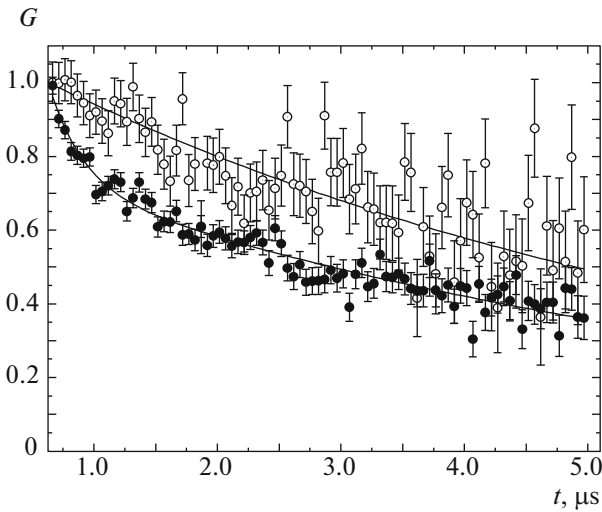


Fig. 7. Relaxation functions $G_i(t)$ at the temperature $2T = 37.5$ K in the (open circles) RUN1 and (closed circles) RUN2 regimes.

45 K in ECMO is caused by a change in the state of Mn^{3+} – Mn^{4+} ferromagnetic pairs in the regions of phase separation rather than by a change in the hyperfine interaction in the basic antiferromagnetic matrix. The doped crystal in this temperature range includes the regions of phase separation whose volume is much smaller than the volume of the initial crystal but is much larger than this volume in EMO. As was mentioned above, the regions of phase separation in ECMO at temperatures below 35 K have the form of 1D superlattices with alternating conducting ferromagnetic and insulating layers according to [10, 11]. Conducting ferromagnetic layers are layers with a 2D electron gas where de Haas–van Alfvén oscillations were observed at temperatures $T < 30$ – 35 K [8, 9]. Fast-relaxation regions can be referred to layers with the 2D electron gas. Indeed, a high density of free electrons in such layers should enhance the relaxation of muons owing to multiple fast recharging: $\mu^+ + e^- \rightarrow \text{Mu} \rightarrow \mu^+ + e^- \rightarrow \text{Mu}$. The depolarization of muons increases strongly because of the scattering of electrons from the muonium on free carriers [15]. This effect in EMO should be much weaker.

The significant difference in temperature behavior of the parameters of the relaxation function for the ECMO sample in the temperature range of 25–40 K in the regimes RUN1 (RUN3) and RUN2 is caused by the process of cooling (heating) of the sample: the phase transition temperature $T_N = 42.5$ K was passed slowly in the regimes RUN1 and RUN3, whereas this temperature was passed rapidly in the RUN2 regime. As a result, there is a noticeable difference in the relaxation functions $G(t)$ in the temperature range of 25–45 K (Fig. 7).

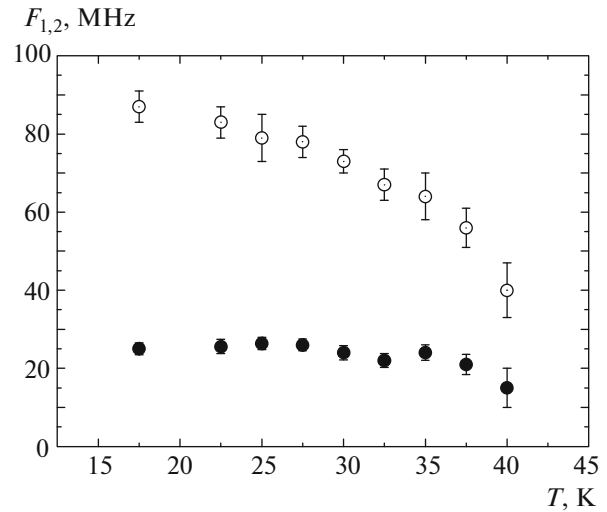


Fig. 8. Temperature dependences of the two observed precession frequencies (closed circles) F_1 and (open circles) F_2 of the muon spin for the ECMO sample measured in the RUN2 regime.

The irreversible character of a change in the magnetization in ECMO at a change in the temperature and magnetic field was also observed in [9]. According to [8, 9], a 1D superstructure of alternating layers of the initial paramagnetic insulating crystal and conducting ferromagnetic layers, which fill the entire sample at $T > 180$ – 200 K, appear in ECMO. As a result, a higher conductivity is conserved in the regions of phase separation at low temperatures at the fast cooling as compared to slow cooling. This increases the relaxation rate of the polarization of muons. The temperature variation regime in [8, 9] corresponded to the regime RUN2 in this work.

We now consider the static part of the G function. The muon spin precession frequency $\Omega_i = 2\pi F_i$ is proportional to the average internal magnetic field $B_i = \Omega_i/\gamma$ at the point of muon localization (here, $\gamma = 13.5544$ kHz/G is the gyromagnetic ratio for the muon). Figure 8 shows the temperature dependence of two observed muon-spin precession frequencies F_1 and F_2 in the regime RUN2 for ECMO. The frequency F_1 is independent of the temperature within the errors up to $T = 35$ K. The frequency F_2 increases with a decrease in the temperature according to the Curie–Weiss law $F_2 \sim (1 - T/T_N)^\beta$, where $T_N = 42.5$ K and $\beta = 0.29 \pm 0.02$, which noticeably differs from a similar exponent $\beta = 0.39 \pm 0.01$ that was determined in [12] for the EMO sample and is characteristic of Heisenberg antiferromagnets.

The weights of the frequencies F_1 and F_2 and their spread in the temperature range of 30–40 K are approximately identical; i.e., $a_1/a_0 \approx a_2/a_0$ and $\Delta_1 \approx \Delta_2$. However, the contributions a_1 and a_2 and the average

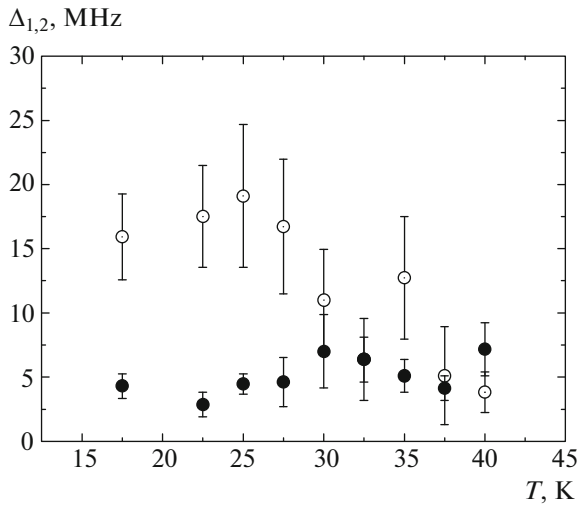


Fig. 9. Temperature dependence of standard deviations (closed circles) Δ_1 and (open circles) Δ_2 for two observed muon-spin precession frequencies in the ECMO sample measured in the RUN2 regime.

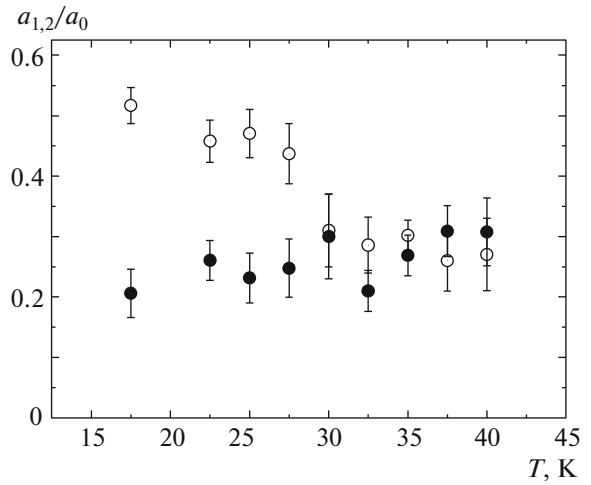


Fig. 10. Relative amplitudes (closed circles) a_1/a_0 and (open circles) a_2/a_0 of the muon-spin precession frequency for the ECMO sample measured in the RUN2 regime.

frequency spreads Δ_1 and Δ_2 are noticeably different at temperatures below 30 K (see Figs. 9 and 10).

The frequency F_2 refers to the basic antiferromagnetic matrix of ECMO. A significant difference of the coefficient β in ECMO from that in EMO [12] indicates a difference in the temperature behavior of their magnetic subsystems. The doping of the sample enhances the frustration of the antiferromagnetic order in the initial matrix in ECMO as compared to EMO. As a result, the critical exponents for the muon-spin precession frequencies are different for the basic matrices in ECMO and EMO. The frequency F_1 refers to the regions of phase separation containing $\text{Mn}^{3+}-\text{Mn}^{4+}$ ferromagnetic ion pairs and e_g electrons recharging them. Noticeable differences between the contributions a_1 and a_2 and between the frequency spreads Δ_1 and Δ_2 (see Figs. 9 and 10) are attributed to a change in the state of the phase-state region near $T=30$ K. Indeed, the intensities of ferromagnetic resonances from the layers of 1D superlattices in the doped crystal decrease sharply when approaching $T=30$ K [10, 12] and the magnetoresistance changes sign [9]. This behavior is attributed to the variation of the charge carrier density in the layers of superlattices at a change in the type of the prevailing conductivity from tunneling to hopping one. The enhancement of the hopping conductivity from the layers of 1D superlattices is responsible for a change in their structure and for an increase in the conductivity in layers with the maximum barriers at these boundaries. In view of this circumstance, it becomes clear why regions in the ECMO sample responsible for the enhanced relaxation and depolarization of muons are observed just in the temperature range of 25–40 K (Figs. 3–6).

4. CONCLUSIONS

The relaxation of the polarization of muons has been comparatively studied in EMO and ECMO ceramic samples. It has been found that the doping of the sample slightly reduces the temperature of the magnetic phase transition from $T_N = 45$ K for the EMO sample to $T_N = 42.5$ K for the ECMO sample. Two precession frequencies of the magnetic moment of the muon in the internal magnetic field have been detected in the ECMO sample. The temperature dependence of the higher frequency referring to the basic antiferromagnetic matrix follows the Curie–Weiss law with the exponent $\beta = 0.29 \pm 0.02$, which differs from the value $\beta = 0.39$ characteristic of 3D Heisenberg magnetics (previously observed in the EMO sample). This is due to the doping of the sample responsible for the enhancement of frustration of its structure. The lower frequency refers to limited regions of phase separation (1D superlattices) where the dynamically equilibrium state is due to the balance of strong interactions (double exchange, Jahn–Teller interaction, and Coulomb repulsion) and is almost independent of the temperature at $T < 30-35$ K. The variation of this frequency at $T > 30-35$ K is initiated by a change in the type of the prevailing conductivity (from tunneling to hopping), which results in a change in the structure of regions of phase separation. Almost identical fast losses (about 20%) of the polarization of muons below the magnetic-ordering temperature T_N have been revealed in both samples. This effect is due to the presence of $\text{Mn}^{3+}-\text{Mn}^{4+}$ ferromagnetic ion pairs and e_g electrons recharging them both along the b axis in the basic antiferromagnetic matrix and in limited regions of phase separation filling a small fraction of the samples at temperatures below T_N . The ther-

malization of muons near such ion pairs is accompanied by the formation of $(\text{Mn}^{4+}-\text{Mn}^{4+}-\text{Mu})$ ferromagnetic complexes, which enhances the loss of polarization of muons. Doping in the ECMO sample increases the volume filled with the regions of phase separation but partially destroys the charge order along the b axis in the basic antiferromagnetic matrix of the sample; as a result, polarization losses in both studied samples are close to each other.

The difference in the temperature behavior of the relaxation of the polarization of muons at different regimes of cooling and heating in the temperature range of 25–45 K has been detected in the ECMO sample. The appearance of a fast-relaxation phase at these temperatures is the most pronounced in the regime of fast cooling to temperatures below the magnetic ordering temperature. This is due to a change in the state of the regions of phase separation (1D superlattices) at a change in the prevailing type of conductivity.

ACKNOWLEDGMENTS

The work of the authors from the Ioffe Institute was supported by the Government of the Russian Federation (project no 14.V25.31.0025).

REFERENCES

1. N. Hur, S. Park, P. A. Sharma, J. S. Ahn, S. Guba, and S.-W. Cheong, *Nature (London)* **429**, 392 (2004).
2. Y. Noda, H. Kimura, M. Fukunaga, S. Kobayashi, I. Kagomiya, and K. Kohn, *J. Phys.: Condens. Matter* **20**, 434206 (2008).
3. P. G. Radaelli and L. C. Chapon, *J. Phys.: Condens. Matter* **20**, 434213 (2008).
4. J. van den Brink and D. I. Khomskii, *J. Phys.: Condens. Matter* **20**, 434217 (2008).
5. V. Baledent, S. Chattopadhyay, P. Fertey, M. B. Lepe-
tit, M. Greenblatt, B. Wanklyn, F. O. Saouma,
J. I. Jang, and P. Foury-Leylekian, *Phys. Rev. Lett.* **114**, 117601 (2015).
6. L. P. Gor'kov, *Phys. Usp.* **41**, 589 (1998).
7. M. Yu. Kagan and K. I. Kugel', *Phys. Usp.* **44**, 553 (2001).
8. V. A. Sanina, E. I. Golovenchits, V. G. Zalesskii,
S. G. Lushnikov, M. P. Scheglov, S. N. Gvasaliya,
A. Savvinov, R. S. Katiyar, H. Kawaji, and T. Atake,
Phys. Rev. B **80**, 224401 (2009).
9. V. A. Sanina, E. I. Golovenchits, V. G. Zalesskii, and
M. P. Scheglov, *J. Phys.: Condens. Matter* **23**, 456003 (2011).
10. E. I. Golovenchits, V. A. Sanina, and V. G. Zalesskii,
JETP Lett. **95**, 386 (2012).
11. V. A. Sanina, E. I. Golovenchits, and V. G. Zalesskii,
J. Phys.: Condens. Matter **24**, 346002 (2012).
12. S. I. Vorob'ev, E. I. Golovenchits, V. P. Koptev,
S. A. Kotov, E. N. Komarov, V. A. Sanina, and
G. V. Shcherbakov, *JETP Lett.* **91**, 512 (2010).
13. S. I. Vorob'ev, A. L. Getalov, E. I. Golovenchits,
V. P. Koptev, S. A. Kotov, E. N. Komarov, I. I. Pav-
lova, V. A. Sanina, and G. V. Shcherbakov, *Phys. Solid
State* **55**, 466 (2013).
14. S. G. Barsov, S. I. Vorob'ev, V. P. Koptev, S. A. Kotov,
S. M. Mikirtych'yants, and G. V. Shcherbakov,
Instrum. Exp. Tech. **50**, 750 (2007).
15. V. P. Smilga and Yu. M. Belousov, *The Muon Method in
Science* (Nauka, Moscow, 1991; Nova Science, NY,
1984).

Translated by R. Tyapaev